




RESEARCH ARTICLE | JANUARY 03 2023


Effect of internal solitary wave on the dynamic response of a flexible riser

Jinlong Duan ; Xu Wang; Jifu Zhou  ; Yunxiang You



Physics of Fluids 35, 017107 (2023)


<https://doi.org/10.1063/5.0130822>



Physics of Fluids

Special Topic: K. R. Sreenivasan:
A Tribute on the occasion of his 75th Birthday

[Submit Today](#)



Effect of internal solitary wave on the dynamic response of a flexible riser

Cite as: Phys. Fluids **35**, 017107 (2023); doi: [10.1063/5.0130822](https://doi.org/10.1063/5.0130822)

Submitted: 15 October 2022 · Accepted: 5 December 2022 ·

Published Online: 3 January 2023



View Online



Export Citation



CrossMark

Jinlong Duan,¹  Xu Wang,¹ Jifu Zhou,^{1,2,a)}  and Yunxiang You³

AFFILIATIONS

¹CAS Key Laboratory for Mechanics in Fluid Solid Coupling Systems, Institute of Mechanics, Beijing 100190, China

²School of Engineering Sciences, University of Chinese Academy of Sciences, Beijing 100049, China

³State Key Laboratory of Ocean Engineering, Shanghai Jiao Tong University, Shanghai 200240, China

^{a)}Author to whom correspondence should be addressed: zhoujf@imech.ac.cn

ABSTRACT

Dynamic responses can arise when a flexible riser encounters the internal solitary wave (ISW) in the ocean. It is, thus, necessary to explore its dynamical behaviors induced by ISW. First, the governing equations of the flexible riser, ISW, and hydrodynamic force are introduced and interpreted. The accordant validations are performed so as to examine the accuracy of the applied models. Then, the dynamic response of the flexible riser is studied with the increase of the nondimensional ISW amplitude. Representative characteristics, such as vortex-induced vibration (VIV), top tension, and stress along the flexible riser, are mainly analyzed and discussed. The results prove that with the propagation of ISW, VIV in both inline (IL) and crossflow (CF) directions can be incurred. The maximum values of IL and CF oscillation frequencies, top tension, inline deflection, as well as riser stress can be detected while the ISW trough reaches to the flexible riser. Furthermore, all these four dynamic characteristics show an increasing trend with the increase of the nondimensional ISW amplitude. Note that the maximum values of oscillation frequencies, inline deflection, and stress on the upper section of the flexible riser tend to be larger compared with those on the lower section. In addition, the maximum inline deflection, top tension, and stress along the flexible riser can be affected by VIV responses.

Published under an exclusive license by AIP Publishing. <https://doi.org/10.1063/5.0130822>

I. INTRODUCTION

Due to the interaction between internal tides and complicated submerged topography, internal solitary wave (ISW) can be generated in a density-stratified ocean. It is reported that such ISW has been frequently detected in the South China Sea.^{1–5} Moreover, ISW with extra-large amplitudes up to more than 200 m has been recorded by previous field observations,^{6–9} which can lead to strongly varying current between its upper and lower water layers. As ISW propagates across marine structures, such as offshore platforms, riser systems, and artificial structures, hydrodynamic loads can be exerted on them. Particularly, the dynamic response of marine risers under the action of ISW is intensive, which can have a severe impact on the pipeline configuration, structural strength, operational efficiency, and safety. Moreover, accidents induced by ISW can occur, thereby threatening the safety of marine engineering and submarines.^{4,9,10} As ISW can appear frequently in deep ocean, it is of great significance to focus on the interaction between marine structures and ISW thoroughly and comprehensively so that references can be offered for the design of marine structures applied for resource exploitation.

For decades, not only the generation, propagation, and transformation of ISW have engrossed many scholars' attention,^{11–17} but also the effect of ISW on marine structures has been investigated based on experimental, numerical, and theoretical approaches.^{18–25} For instance, by considering the combination of the Korteweg–de Vries (KdV) model and Morison formula, the forces and torques acting on vertical cylinders by ISW have been calculated by Cai *et al.*^{26,27} In addition, the hydrodynamic force induced by ISW was also estimated by other researchers by combining Morison formula and other ISW theories.^{28–32} Similarly, the hydrodynamic force on one or two cylinders induced by ISW has been examined by many researchers experimentally and numerically, wherein the force exerted on one and two cylinders was mainly studied.^{33–36} It is found that the distance between two cylinders can have an impact on hydrodynamic interactions between ISW and structures. The force of oblique ISW on slender bodies was also experimentally researched by Wang *et al.*,³⁷ in which the strong shear effect caused by ISW was mainly focused. Moreover, experiments have been conducted to investigate the inline (IL) and transverse forces induced by ISW on semisubmersible platforms by

Chen *et al.*,^{23,38} indicating that the force acting on marine structures is sensitive to the propagation direction of ISW. It is also proved by Cui *et al.*³⁹ and Cheng *et al.*⁴⁰ that the mooring tensions of a platform can be affected when ISW propagates across it. In addition to the aforesaid works, contributions to investigate the characteristics of interaction between ISW and marine structures can also be found in other literatures,^{41–45} which has provided practical and meaningful references for the design of marine structures in ocean engineering.

With large aspect ratios, marine risers can inevitably undergo ISW during deep sea resource exploitation. Hence, it is imperative to study the dynamic response of marine risers undergoing ISW so as to guarantee the safety of deep sea resource exploitation equipment. Recently, some research on the interaction between ISW and marine risers has emerged. It is found by Zhang *et al.*,⁴⁶ Guo *et al.*,⁴⁷ and Lou and Yu⁴⁸ that the ISW plays a dominated role in affecting the dynamics of a marine riser regardless of background current. While ISW propagates across a connected drilling riser, the impact of ISW on the riser under combined loads of ocean currents, surface waves, and ISW have been evaluated by Deng *et al.*⁴⁹ The envelopes of riser properties in the upper seawater layer and the horizontal deviation of a hang-off riser bottom were found dramatically increased under the effect of ISW by Fan *et al.*⁵⁰ In addition, many other studies have further revealed the dynamic response of marine riser systems with consideration of the ISW effect.^{51–54}

Although the interaction between ISW and riser systems has been studied by many scholars recently, these works mainly focus on the riser deflection and stress variation in the inline direction rather than vortex-induced vibration (VIV). As concerned, the corresponding current can be generated with the propagation of ISW. When the vortex shedding frequency is locked on the natural frequency of a flexible riser, VIV can be easily triggered, thereby posing a threat on the riser safety. Therefore, the dynamic response, including inline deflection, VIV response, stress, and other terms, should be paid attention when the interaction between ISW and the riser system is investigated. In addition, most of experimental and numerical studies concentrate on dynamics of risers with certain scale ratio, rather than full-scale risers. Hence, the objective of this study is to investigate the dynamic response of a full-scale tensioned flexible riser with considering the effect of the nondimensional ISW amplitude. The paper is structured as follows. First, the eKdV equation used to simulate the flow field of ISW as well as the time-domain structural and hydrodynamic models applied to calculate VIV responses of a flexible riser are interpreted in Sec. II. Then, validations are carried out to guarantee the accuracy of the ISW generation model. In Sec. III, the dynamic response of a full-scale flexible riser under actual ISW is investigated with considering the effect of the nondimensional ISW amplitude, including the inline (IL) and crossflow (CF) VIV responses, top tension, and stress along the flexible riser. Finally, conclusions are drawn in Sec. IV.

II. MODELING METHOD

A. The flexible riser model

A simply supported flexible riser subjected to ISW is illustrated in Fig. 1. The Euler–Bernoulli beam theory is used to model the flexible riser undergoing ISW in our study. Correspondingly, the governing equations of the flexible riser can be written as

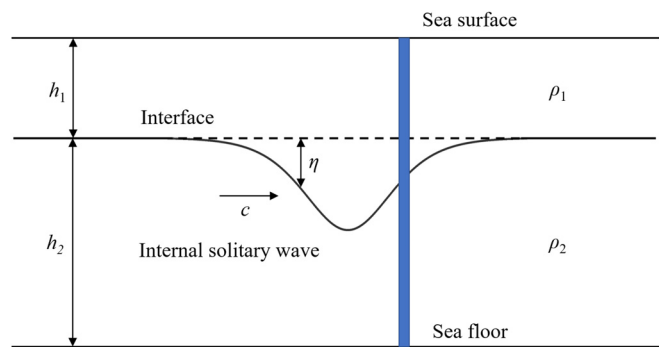


FIG. 1. Sketch of a flexible riser subjected to ISW.

$$m \frac{\partial^2 x(z, t)}{\partial t^2} + c \frac{\partial x(z, t)}{\partial t} - T \frac{\partial^2 x(z, t)}{\partial z^2} + EI \frac{\partial^4 x(z, t)}{\partial z^4} = F_{IL}(z, t), \tag{1}$$

$$m \frac{\partial^2 y(z, t)}{\partial t^2} + c \frac{\partial y(z, t)}{\partial t} - T \frac{\partial^2 y(z, t)}{\partial z^2} + EI \frac{\partial^4 y(z, t)}{\partial z^4} = F_{CF}(z, t), \tag{2}$$

where m denotes the riser mass per unit length; c is the structure damping, which can be calculated based on the Rayleigh damping model; EI and T are the bending stiffness and top tension, respectively; $x(z, t)$ and $y(z, t)$ denote the dimensional displacements in IL and CF directions; and $F_{IL}(z, t)$ and $F_{CF}(z, t)$ represent the IL and CF hydrodynamic forces caused by ISW. Then, the finite element method is utilized to discretize the IL and CF governing equations of the flexible riser. The Newmark- β method is employed to solve the discretized equations. Correspondingly, the dynamic response of the flexible riser subjected to ISW can be examined and investigated.

B. The ISW generation model

An extended Korteweg–de Vries (eKdV) equation is adopted for the simulation of ISW.^{55,56} Compared with Korteweg–de Vries (KdV) equation, a cubic nonlinear term is added in eKdV equation in order to predict the profile of ISW accurately. Therefore, the eKdV equation is used here and as follows:

$$\frac{\partial \zeta}{\partial t} + (c_0 + \alpha_1 \zeta + \alpha_2 \zeta^2) \frac{\partial \zeta}{\partial x} + \beta \frac{\partial^3 \zeta}{\partial x^3} = 0. \tag{3}$$

Under the two-layer approximation, the wave phase speed c_0 , the coefficients of quadratic nonlinearity α_1 , cubic nonlinearity α_2 , and dispersion β in the eKdV equation are given by

$$c_0 = \sqrt{g \frac{h_1 h_2 (\rho_2 - \rho_1)}{\rho_1 h_2 + \rho_2 h_1}}, \tag{4}$$

$$\alpha_1 = -\frac{3c_0}{2} \frac{\rho_1 h_2^2 - \rho_2 h_1^2}{\rho_1 h_1 h_2^2 + \rho_2 h_2 h_1^2}, \tag{5}$$

$$\alpha_2 = \frac{3c_0}{h_1^2 h_2^2} \left[\frac{7}{8} \left(\frac{\rho_1 h_2^2 - \rho_2 h_1^2}{\rho_1 h_2 + \rho_2 h_1} \right)^2 - \frac{\rho_2 h_1^3 + \rho_1 h_2^3}{\rho_1 h_2 + \rho_2 h_1} \right], \tag{6}$$

$$\beta = \frac{c_0(\rho_1 h_1 h_2^2 + \rho_2 h_2 h_1^2)}{6(\rho_1 h_2 + \rho_2 h_1)}. \tag{7}$$

The solution of eKdV equation can be written as

$$\zeta = \frac{a}{B + (1 - B)\cosh^2[\lambda_{eKdV}(x - c_{eKdV}t)]}, \tag{8}$$

where a denotes the amplitude of ISW, and

$$c_{eKdV} = c_0 + \frac{a}{3} \left(\alpha_1 + \frac{1}{2} \alpha_2 a \right), \tag{9}$$

$$\lambda_{eKdV}^2 = \frac{a(2\alpha_1 + \alpha_2 a)}{24\beta}, \tag{10}$$

$$B = \frac{-\alpha_2 a}{2\alpha_1 + \alpha_2 a}. \tag{11}$$

Accordingly, the velocity induced by ISW can be obtained based on eKdV equation, which can be applied to calculate the hydrodynamic force exerted on the flexible riser.

C. The hydrodynamic force model

The hydrodynamic forces acting on the flexible riser undergoing ISW is calculated based on the hydrodynamic force model proposed in the works of Duan *et al.*^{57,58} Likewise, the inertia force, the drag force in the IL direction, and the vortex-induced force in CF and IL directions are considered for the hydrodynamic force induced by ISW. As the applied hydrodynamic force model has been elaborated in detail in the works of Duan *et al.*,⁵⁷⁻⁶⁰ it will be reinterpreted briefly here. The hydrodynamic force F_{IL} in the IL direction and F_{CF} in the CF direction are given as

$$F_{IL} = \frac{\rho\pi D^2}{4} \left[C_M \frac{\partial u(z, t)}{\partial t} - (C_M - 1) \frac{\partial^2 x(z, t)}{\partial t^2} \right] + F_D + F_{vor, IL}, \tag{12}$$

$$F_{CF} = -\frac{\rho\pi D^2}{4} C_a \frac{\partial^2 y(z, t)}{\partial t^2} + F_{vor, CF}, \tag{13}$$

where the inertia force, the drag force F_D , and the IL vortex-induced force $F_{vor, IL}$ are included for F_{IL} , while the hydrodynamic force F_{CF} in the CF direction can be decomposed into the inertia force and the CF vortex-induced force $F_{vor, CF}$. The added mass coefficient $C_M = 2.0$ is applied for F_{IL} due to the variation of flow velocity in the IL direction. ρ and D represent the flow density and external riser diameter. As for the hydrodynamic force in the CF direction, the value $C_a = 1.0$ is utilized with the absence of flow velocity variation in the CF direction.

As the current induced by ISW is time-varying, the excitation or damping regions of the flexible riser corresponding to the instantaneous flow velocity need to be identified at each time step so that corrective hydrodynamic force can be obtained and exerted on the flexible riser subjected to ISW. Furthermore, the excitation hydrodynamic coefficient C_L used to calculate the excitation hydrodynamic force is also determined at each time step. Then, the hydrodynamic force on the flexible riser, either excitation or damping forces, can be acquired. Since the same method of identifying excitation and damping regions as well as selecting the appropriate hydrodynamic coefficient is utilized as those in the works of Duan *et al.*,⁵⁷ it will not be reinterpreted in detail here. After the hydrodynamic forces in both IL

and CF directions are calculated at each time step, the dynamic response of the flexible riser undergoing ISW can be obtained by coupling with the structural governing equations.

III. VALIDATIONS

Before investigation on the dynamic response of a flexible riser subjected to ISW, the validation of the applied models needs to be carried out, including the models of ISW generation, hydrodynamic forces, and structural response. It should be mentioned that the structural and hydrodynamic force models employed here have carefully been validated based on the comparison of numerical results and experimental data by Duan *et al.*⁵⁷⁻⁶⁰ under uniform flow, shear flow, as well as oscillatory flow. It has been proved that VIV response of a flexible riser under various environmental conditions can be accurately captured. Therefore, the validations of structural and hydrodynamic force models will not be performed again here. Since the code of ISW generation is newly developed during our investigation, it is necessary to examine the accuracy of this model. Correspondingly, some characteristics of ISW are simulated based on the eKdV theory and then compared with the experimental data provided by Grue *et al.*⁵⁶ The wave amplitude and maximum velocity along the water depth are mainly demonstrated with the variation of a depression amplitude a to the upper layer depth h_1 .

As shown in Fig. 2, the simulated ISW amplitudes show a good agreement with the experimental ones with $a/h_1 = 0.22, 0.36,$ and 0.91 . It can be clearly observed that the maximum values of wave amplitudes in all three cases can be precisely captured by the eKdV equation. Regarding to the horizontal velocity of the ISW flow field, the numerical and experimental results in both upper and lower layers can match each other very well, as displayed in Fig. 3. Therefore, it can be concluded that the code developed for our investigation is reliable

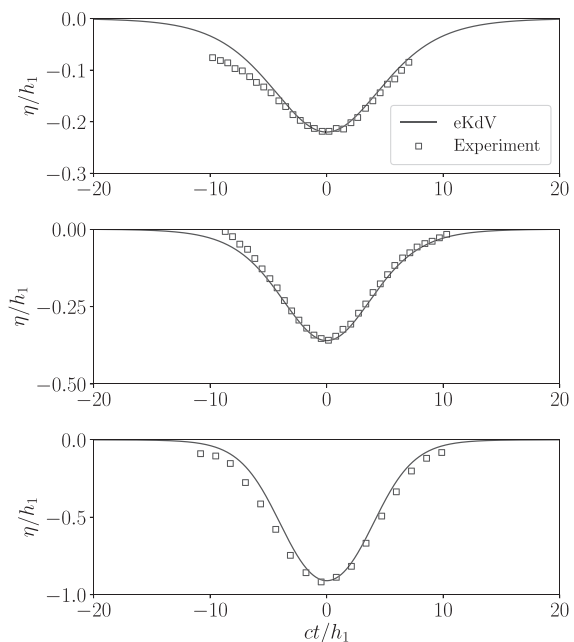


FIG. 2. Comparison of ISW wave forms with different values of a/h_1 (upper: $a/h_1 = 0.22$; middle: $a/h_1 = 0.36$; and bottom: $a/h_1 = 0.91$).

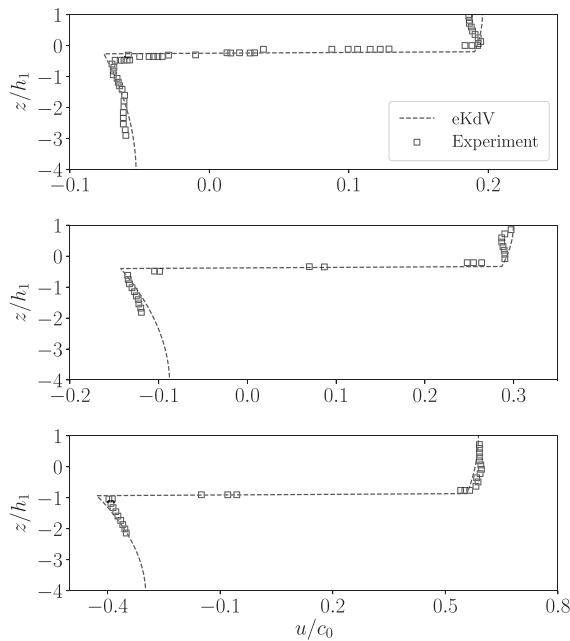


FIG. 3. Comparison of the maximum horizontal velocity by ISW with different values of a/h_1 . (upper: $a/h_1 = 0.22$; middle: $a/h_1 = 0.36$; and bottom: $a/h_1 = 0.91$).

and can reproduce main profiles of ISW. Then, the dynamic response of a flexible riser undergoing ISW is investigated based on the afore-said three models.

IV. RESULTS AND DISCUSSION

In this section, the dynamical behaviors of the flexible riser subjected to ISW with various amplitudes are mainly investigated and analyzed, including VIV responses in both IL and CF directions, top tension, and riser stress. The corresponding parameters of the full-scale flexible riser and ISW are presented in Tables I and II. Note that the amplitude of ISW can be nondimensionalized by $\alpha = a/H$, where a is the ISW amplitude and H denotes an intrinsic vertical scale.⁵⁵ Here, the upper layer depth h_1 is chosen as the scale for the nondimensional ISW amplitude. Correspondingly, the nondimensional ISW amplitude $\alpha = 0.1, 0.2, 0.3, 0.4, \text{ and } 0.5$ during our investigation.

A. The flow field of ISW

Based on the eKdV equation, the flow field induced by ISW with $\alpha = 0.5$ is obtained and illustrated in Fig. 4, wherein the red vectors

TABLE I Parameters of the flexible riser model.

Parameter	Value
Length L (m)	1000
Young’s elasticity module E (Pa)	2.1×10^{11}
Outer diameter D (m)	0.25
Inner diameter d (m)	0.2
Density ρ (kg m^{-3})	7850
Pretension T (kN)	1000

TABLE II. Parameters of ISW generation.

Parameter	Value
Depth of the upper layer h_1 (m)	300
Depth of the lower layer h_2 (m)	700
Density of the upper layer ρ_1 (kg m^{-3})	998
Density of the lower layer ρ_2 (kg m^{-3})	1025
ISW amplitude a (m)	30, 60, 90, 120, 150

represent the velocities in the upper and lower layers, while the blue line denotes the waveform of ISW. It can be observed that the induced velocity in the upper layer shares a same direction with the propagation of ISW. By contrast, the velocity direction in the lower layer is opposite to that of the upper ones. Furthermore, large values of incurred velocity in both upper and lower layers occur nearly at the ISW trough, accompanied by the upper ones slightly larger than the lower one, as observed in Fig. 4. The velocity field here also manifests the strongly shear characteristics of the ISW flow field, which should be paid attention during the investigation on the responses of the flexible riser. In addition, the maximum velocity along the water depth is also calculated with the increase in the nondimensional ISW amplitude, as shown in Fig. 5. Obviously, the maximum value of the induced velocity shows an increasing trend when the nondimensional ISW amplitude is enhanced, which can be attributed to more energy due to large ISW amplitude. Then, the effect of the nondimensional ISW amplitude on the dynamic response of the flexible riser is studied based on such ISW model.

B. Time-dependent VIV responses

First, representative VIV characteristics in both IL and CF directions, including the time history of vibration, its corresponding excited mode, and frequency at node 400, are analyzed and depicted in Figs. 6 and 7 when the flexible riser undergoes ISW with different amplitudes. It should be mentioned that VIV features are demonstrated after removing inline deflection here in order to reveal the effect of the non-dimensional ISW amplitude on IL and CF VIV responses more specifically.

Obviously, VIV responses are triggered for the flexible riser in both IL and CF directions with the propagation of ISW. When ISW has not arrived at the flexible riser, no VIV occurs due to the absence of induced velocity in the fluid. As ISW propagates toward the flexible

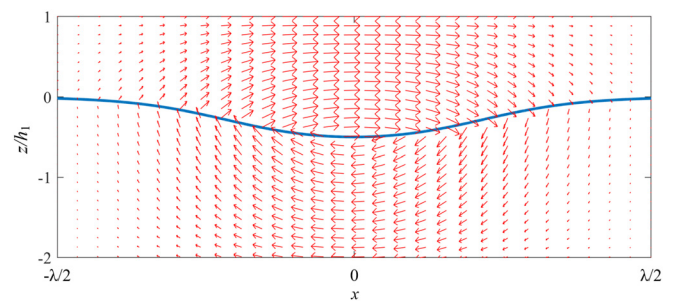


FIG. 4. The flow field induced by ISW with $\alpha = 0.5$.

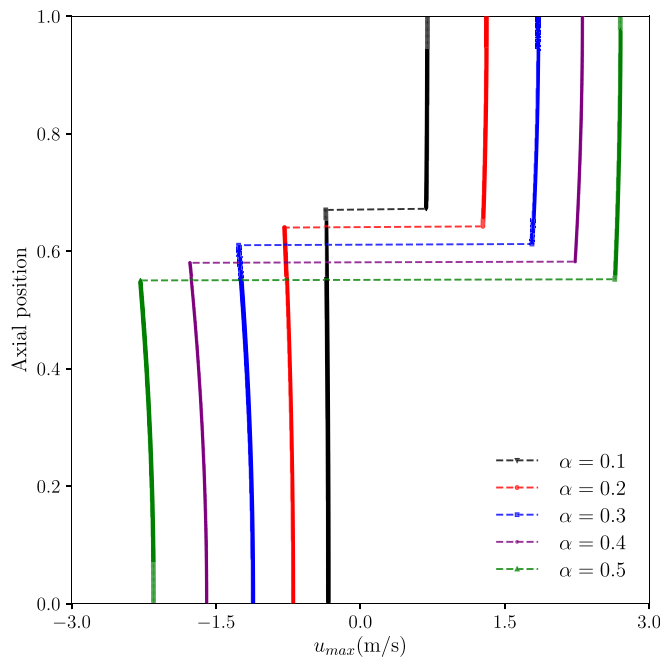


FIG. 5. The maximum velocity along the water depth induced by ISW with various nondimensional amplitudes.

riser, there appears flowing current acting on the structure, leading to the occurrence of IL and CF VIV gradually, as shown in Figs. 6 and 7. As a result, vibration frequencies corresponding to low mode responses begin to emerge in both IL and CF directions regardless of the nondimensional ISW amplitude, which can be attributed to the low induced velocity by ISW. With the propagation of ISW, the incurred velocity is increased gradually, thereby causing that high mode IL and CF VIV responses are excited. Therefore, high-frequency VIV responses can be detected when the trough of ISW is approaching to the flexible riser gradually. As the ISW trough arrives at the flexible riser, maximum values of induced velocity along the flexible riser can be induced. Consequently, highest IL and CF vibration frequencies accordant to high mode VIV responses appear due to the maximum incurred velocity, as observed in Figs. 6 and 7. When ISW passes across the flexible riser, the vibration frequency as well as the excited mode of VIV in both IL and CF directions shows a decreasing trend, which can be ascribed to the reduction of the induced velocity by ISW. While ISW continues to move away from the flexible riser, IL and CF VIV responses almost disappear.

In addition, it can be observed that two or more frequencies can be detected for IL and CF VIV responses simultaneously. This is because the velocity induced by ISW along the flexible riser is various rather than uniform. As demonstrated in Figs. 4 and 5, current velocities with opposite directions and various values can be incurred by ISW in upper and lower layers, respectively, and the values of induced velocity tend to be larger near the ISW trough. As a consequence, two or more modes of VIV responses can be excited along the flexible riser due to the different induced velocities. Accordingly, two or more oscillation frequencies can be detected for IL and CF VIV responses, as seen in Figs. 6 and 7.

Nonetheless, it should be noticed that hysteresis phenomenon can be also detected for VIV incurred by ISW regardless of the nondimensional amplitude, as demonstrated in Figs. 6 and 7. As ISW propagates toward or passes across the flexible riser, current velocities with equal values can be induced in these two processes. Theoretically, VIV amplitudes of the flexible riser subjected to the same current velocity induced by ISW should not show any discrepancies. However, it is found that the IL and CF VIV amplitudes in the deceleration process of velocity induced by ISW are larger compared with those in the velocity acceleration process when ISW propagates toward the flexible riser, which is similar to the findings of Duan *et al.*⁵⁹ and Fu *et al.*⁶¹ The occurrence of VIV hysteresis can be ascribed to the mode transition due to the variation of induced velocity with ISW propagation. With the increase or decrease in the velocity incurred by ISW, different modes of VIV responses determined by certain induced velocities can be triggered, leading to mode jump phenomenon for IL and CF VIV. Although new mode VIV responses occur with the change of the induced velocity, the former excited ones cannot disappear immediately, meaning that the appearance of new mode VIV response is accompanied by the triggered ones decaying slowly. Therefore, multi-mode VIV responses can be detected simultaneously with the propagation of ISW. Meanwhile, the VIV amplitudes are enlarged due to the existence of multi-mode responses. As a consequence, hysteresis phenomenon can arise with the ISW propagation regardless of the nondimensional amplitude. Likewise, when ISW passes away enough from the flexible riser, the occurrence of VIV response in both IL and CF directions can also be explained by the existence of hysteresis. As shown in Figs. 6 and 7, even though the induced velocity by ISW tends to disappear, VIV responses can be still detected for the flexible riser in both IL and CF directions, which should be attributed to the hysteresis effect.

Another notable characteristics worthy attention is the variation of VIV amplitudes in both IL and CF directions with the ISW propagation. Evidently, no vibration occurs when the induced velocity is small enough. With the slow approach of ISW, VIV can be excited. Correspondingly, the flexible riser oscillates with certain amplitudes in IL and CF directions. It should be emphasized that the maximum VIV amplitudes appear not always concurrent with the occurrence of the maximum velocity incurred by ISW. This is because the reduced velocity plays a dominant role in the determination of VIV amplitudes [$U_r = u/(f_n D)$, where u , f_n , and D denote the external flow velocity, the n -order vibration frequency, and external diameter of the flexible riser]. It can be seen that the reduced velocity is mainly affected by the external flow velocity and vibration frequency. Although the induced velocity is increased when the ISW comes toward the flexible riser, the oscillation frequencies are also changed with new mode VIV responses triggered, resulting in the uncertainty of the reduced velocity value. Since the VIV amplitudes are determined by the uncertain reduced velocity, VIV responses with unpredictable amplitudes can be captured in both IL and CF directions with the propagation of ISW, as presented in Figs. 6 and 7.

Although the change in the reduced velocities can be regarded as an important factor responsible for the variation of IL and CF VIV amplitudes, the summation of multi-frequency VIV responses as well as the transient duration of each mode VIV response can play potential roles in the appearance of the unpredicted VIV amplitude. As interpreted above, hysteresis phenomenon occurs due to the

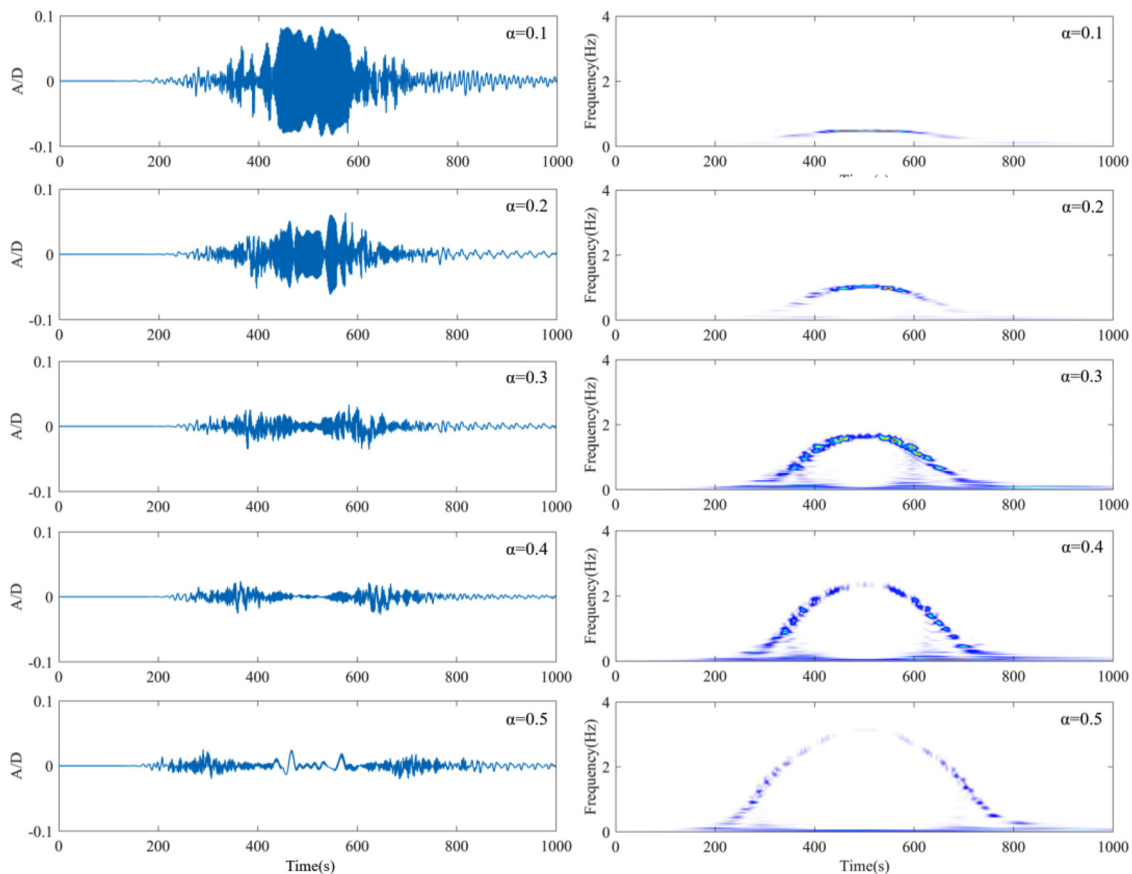


FIG. 6. Time dependent VIV response and frequency distribution in the IL direction with various nondimensional ISW amplitudes (left: time history of VIV and right: VIV frequency distribution with time).

time-varying velocity induced by ISW, resulting in the existence of multi-mode VIV response simultaneously. Consequently, the superposition of the simultaneously existing VIV responses contributes to the variation of the maximum VIV amplitude in IL and CF directions. It should be noticed that the summation of multi-mode response can lead to either enlargement or diminishment of the maximum VIV amplitude, which accounts for the change in the maximum VIV amplitude while the ISW propagates. In addition, the change of VIV amplitudes can be also impacted by the transient mode jump of VIV response. Since the induced flow velocity varies rapidly with the propagation of ISW, VIV mode transition in both IL and CF directions occurs frequently. As a result, VIV response with certain modes cannot be developed into a relatively steady response entirely, due to the short duration of the triggered VIV mode, thereby leading to the unpredicted VIV amplitudes.

Regarding to the effect of the nondimensional ISW amplitude, it is proved that the excited mode, vibration frequency and amplitude of VIV responses in both IL and CF directions can be impacted, particularly for the former two (Figs. 6 and 7). With the nondimensional ISW amplitude $\alpha = 0.1$, the 23rd and 13th mode VIV responses can be triggered in IL and CF directions, respectively, when the flexible riser is subjected to the maximum velocity induced by ISW.

Correspondingly, the maximum IL and CF oscillation frequency of approximately 1.07 and 0.578 Hz can be detected. As the nondimensional ISW amplitude is increased, the excited mode and vibration frequency of the flexible riser in both IL and CF directions are notably enlarged under the maximum induced velocity by ISW. It can be observed in Figs. 6 and 7 that the 65th and 42nd mode responses with maximum oscillation frequencies of 3.80 and 2.18 Hz are captured for the IL and CF VIV responses while the nondimensional amplitude of ISW is increased up to 0.5. The increase in the excited mode and vibration frequency in IL and CF directions can be explained by the enlargement of the maximum induced velocity due to the amplification of the nondimensional ISW amplitude. Moreover, the IL and CF oscillation amplitudes are also affected by the enlargement of the nondimensional ISW amplitude, which can be seen in Figs. 6, 7, and 11. The changing trend of IL and CF VIV amplitudes with the increase of the nondimensional ISW amplitude will be analyzed and discussed in detail in Sec. IV E.

As discussed above, multi-mode and multi-frequency VIV response can be triggered simultaneously in both IL and CF directions with the propagation of ISW. With the increase of the nondimensional ISW amplitude, multi-mode and multi-frequency IL and CF VIV responses can still be captured for the flexible riser undergoing ISW,

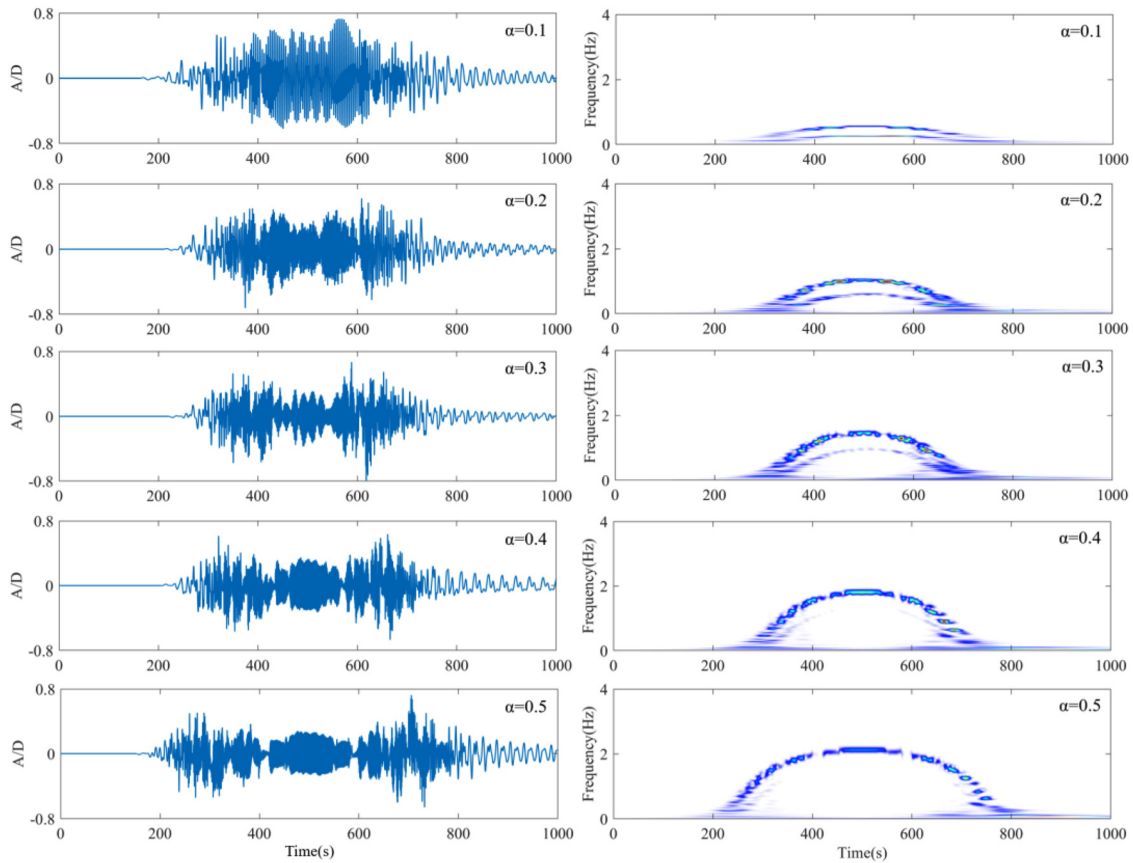


FIG. 7. Time-dependent VIV response and frequency distribution in the CF direction with various nondimensional ISW amplitudes (left: time history of VIV and right: VIV frequency distribution with time).

indicating that the feature of simultaneous multi-mode and multi-frequency VIV is not influenced by the nondimensional ISW amplitude.

C. Oscillation frequency along the flexible riser

The above-mentioned results prove that the increase of the non-dimensional ISW amplitude has a notable effect on IL and CF VIV oscillation frequencies. Therefore, the vibration frequencies long the flexible riser in both IL and CF directions are presented in Figs. 8 and 9 with the nondimensional ISW amplitude variation so as to reveal the impact of the nondimensional ISW amplitude on VIV response comprehensively. The colorful surfaces in Figs. 8 and 9 represent the IL and CF VIV responses along the flexible riser, accompanied by certain oscillation frequency due to the propagation of ISW.

Similarly, the multi-frequency VIV response is evidently detected in both IL and CF directions for the flexible riser subjected to ISW. With the increase of the nondimensional ISW amplitude, high-mode IL and CF VIV responses are triggered due to the enlargement of maximum induced velocity, causing that the flexible riser oscillates with corresponding high IL and CF frequencies. It should be noticed that the detected dominant vibration frequencies on the upper and lower sections of the flexible riser show an obvious disparity regardless of the

nondimensional ISW amplitude. For instance, with the nondimensional ISW amplitude $\alpha = 0.1$, the dominant oscillation frequencies of around 1.07 and 0.474 Hz in the IL direction are detected for the upper and lower sections of the flexible riser, respectively, while these two parts mainly vibrates with predominant frequencies of approximately 0.571 and 0.256 Hz in the CF direction. When the nondimensional ISW amplitude is increased to 0.5, the values of IL and CF dominant vibration frequencies for the upper section of the flexible riser are enhanced to about 3.80 and 2.18 Hz, respectively, and those with values of around 3.13 and 1.74 Hz are captured for the lower section. Such discrepancy between the predominant oscillation frequencies on the upper and lower sections can be attributed to the various current velocities along the flexible riser incurred by ISW. As varied flow velocities are induced along the flexible riser by ISW, different modes of VIV are triggered accordingly, leading to the occurrence of various IL and CF dominant vibration frequencies on the upper and lower sections, respectively. It can also be found that the change of the non-dimensional ISW amplitude has scarcely an effect on the existence of oscillation frequency disparity on the upper and lower sections of the flexible riser, indicating that such characteristics is mainly determined by the remarkably different flow velocities by ISW in the upper and lower layers.

08 April 2024 02:58:45

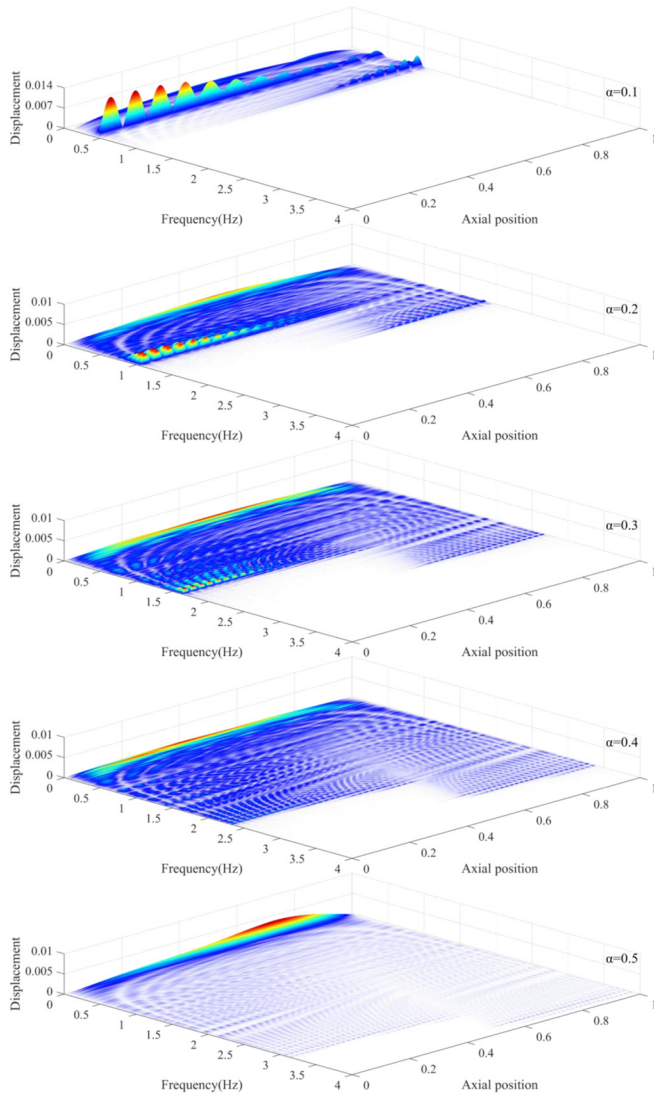


FIG. 8. Oscillation frequency along the flexible riser in the IL direction with various nondimensional ISW amplitudes.

It should also be paid attention that the oscillation frequency bandwidths for IL and CF VIV along the flexible riser are notably widened with the increase of the nondimensional ISW amplitude. Clearly, when the nondimensional ISW amplitude is with a low value, the vibration frequency bandwidths tend to be narrow for both IL and CF VIV responses. As the nondimensional ISW amplitude is increased, the oscillation frequency bandwidths can be remarkably broadened for both IL and CF VIV responses, as demonstrated in Figs. 8 and 9. This is because the enlarged induced flow velocities in upper and lower layers due to the nondimensional ISW amplitude increase account for the augment of the vibration frequency bandwidth for IL and CF VIV. When the nondimensional ISW amplitude is magnified, large flow velocities are incurred accordingly, resulting in more energy transferred into the structure system. Consequently, the IL and CF oscillation frequency bandwidths are widened.

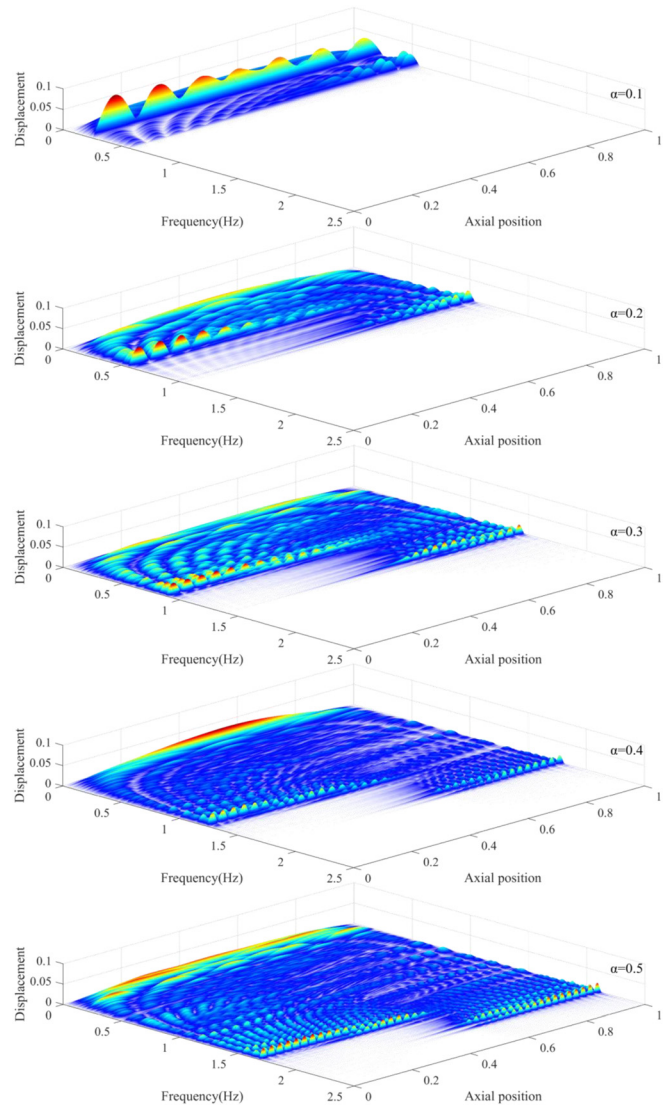


FIG. 9. Oscillation frequency along the flexible riser in the CF direction with various nondimensional ISW amplitudes.

D. Variation of top tension

Since the variation of top tension has been proved closely related to VIV response, especially under unsteady flows,⁶⁰ the time history and frequency distribution of top tension with the increase of the non-dimensional ISW amplitude are analyzed and demonstrated in Fig. 10. Similar to IL and CF VIV response, multi frequencies can be captured for the top tension with the ISW propagation. It can be seen that when the ISW starts to travel toward the flexible riser, the change in the top tension can be hardly detected due to the absence of VIV and inline deflection. With ISW approaching, the values of top tension are gradually increased, which can be ascribed to the occurrence of inline deflection and VIV responses in both IL and CF directions due to the flow velocity incurred by ISW. As shown in Fig. 10, the maximum top tension appears almost concurrent with the ISW trough arriving at the

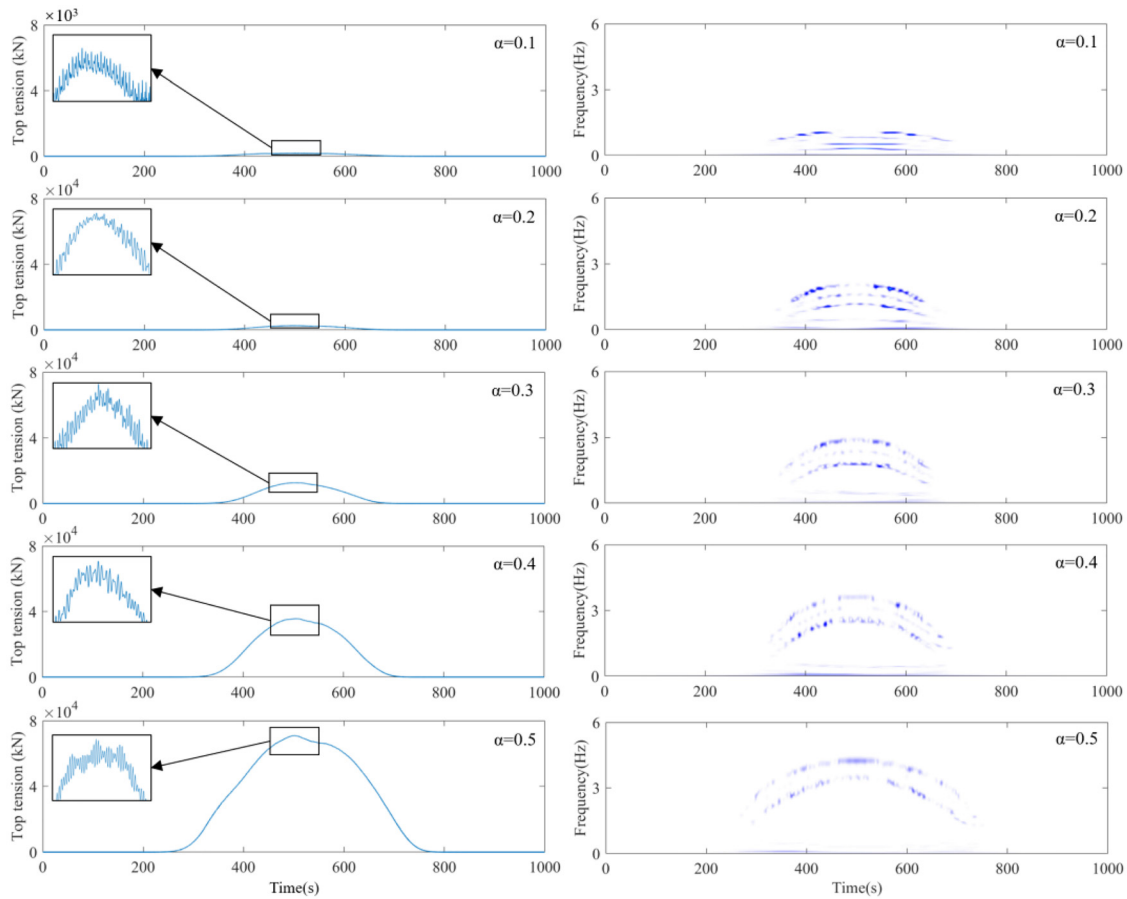


FIG. 10. Variation of top tension with various nondimensional ISW amplitudes (left: time history of top tension and right: top tension frequency distribution with time).

flexible riser regardless of the nondimensional ISW amplitude. While the ISW passes across the flexible riser, the top tension shows a decreasing trend. This is because the reduction of the inline deflection mainly contributes to the decreasing of top tension. When ISW propagates far away, the variation of top tension tends to disappear with the absence of IL and CF VIV responses as well as inline deflection.

It is worthy attention that VIV responses in IL and CF directions can exert an impact on the change of the top tension. Since the top tension variation is mainly focused under the effect of inline deflection with ignorance of VIV response, some characteristics of the top tension cannot be captured, such as vibrations and frequencies related to VIV. During our investigation, it can be observed that VIV responses have an evident effect on the time history and frequency of top tension regardless of the nondimensional ISW amplitude. For instance, when the nondimensional ISW amplitude $\alpha = 0.1$, four vibration frequencies of approximately 0.262, 0.512, 0.924, and 1.03 Hz can be captured for the top tension with the ISW trough passing through the flexible riser, which is mainly related to the VIV frequencies of 0.256, 0.571, 0.985, and 1.07 Hz in both IL and CF directions. The appearance of vibration features proves the influence of IL and CF VIV responses on the top tension, which should not be ignored.

In addition, it can be seen from Fig. 10 that the maximum value of top tension is notably changed with the increase of the nondimensional ISW amplitude. As shown in Fig. 10, the maximum values of top tension with $\alpha = 0.1$ and 0.2 are around 176 and 2.54×10^3 kN, respectively. When the nondimensional ISW amplitude is equal to 0.4 and 0.5 , the maximum top tension values are increased up to approximately 3.56×10^4 and 7.08×10^4 kN. The remarkable enlargement of top tension is mainly attributed to the notable increase of inline deflection due to the induced velocity by ISW. It should be noted that the values of top tension variation induced by VIV responses are noticeably small compared those caused by the inline deflection, implying that the inline deflection mainly plays a dominated role in determining the change of the top tension. In terms of the oscillation frequency of the top tension, it can also be found that with the increase of the nondimensional ISW amplitude, high oscillation frequencies can be detected for the top tension. As shown in Fig. 10, the vibration frequencies of around 3.23 and 3.86 Hz corresponding to the IL and CF VIV responses are obtained for the top tension when the ISW trough reaches to the flexible riser. The enlargement of top tension frequencies with the increase of the nondimensional ISW amplitude can be explained by high oscillation frequencies of VIV responses induced by ISW.

E. Maximum amplitudes of the dynamic response

As the current velocities induced by ISW play a dominated role in the determination of the IL and CF vibration amplitudes as well as inline deflection, it is necessary to investigate the changing trend of these characteristics with the increase of the nondimensional ISW amplitude. Note that the values of inline deflection are remarkably large compared with the VIV oscillation amplitudes, so the results of these two features are analyzed and demonstrated separately here. Hence, the IL and CF vibration amplitudes as well as inline deflections under different values of the nondimensional ISW amplitude are illustrated in Figs. 11 and 12, respectively.

The maximum inline deflection of a flexible riser induced by ISW has widely been studied by many researchers, wherein the value of inline deflection is found increased with the enlargement of the ISW amplitude. Likewise, the maximum inline deflection is also enlarged with the increase in the nondimensional ISW amplitude, which can be explained by the magnification of inline hydrodynamic force exerted on the flexible riser. As illustrated in Fig. 11, when the nondimensional ISW amplitude $\alpha = 0.1$, the maximum inline deflections in the upper and lower layers are about 12.25 and 3.29, respectively. As the nondimensional ISW amplitude is increased up to 0.5, the maximum inline deflections of 177.78 and 156.89 can be detected in the upper and lower layers. This is because the maximum induced velocity is enlarged with the increase in the nondimensional ISW amplitude, causing that larger drag force in the IL direction is exerted on the flexible riser. Consequently, the maximum inline deflection appears due to the increased IL drag force. Note that the maximum inline deflection in the upper layer is always larger than that in the lower layer during our simulation, which can be attributed to the ISW chosen here. That is, large maximum velocity is incurred by ISW in the upper layer compared to that in the lower layer. As a consequence, larger value of maximum drag force is exerted on the upper section of

the flexible riser, leading to larger inline deflection accordingly. In addition, the flexible riser undergoing ISW deflects in the IL direction with opposite directions in the upper and lower layers, which can be ascribed to the opposite velocity induced by ISW.

Since VIV responses in both IL and CF directions can be excited by ISW, the maximum VIV amplitudes are focused with the increase of the nondimensional ISW amplitude. As presented in Fig. 12, the variation of the nondimensional ISW amplitude has an obvious effect on the maximum IL amplitude, while the maximum VIV amplitude in the CF direction is scarcely changed. It can be seen that the maximum VIV amplitude in the IL direction almost shows a decreasing trend with the increase of the nondimensional ISW amplitude, which can be mainly ascribed to the variation of current velocities incurred by ISW. As the nondimensional ISW amplitude is enhanced, the induced velocity is changed, leading to the variation of reduced velocity. Accordingly, the VIV amplitude in the IL direction is descended with the increase of the nondimensional ISW amplitude. Another potential factor is that the energy allocation on the dynamic response of the flexible riser in IL direction, mainly including IL VIV and inline deflection, might lead to the reduction of IL VIV amplitudes. As discussed above, the inline deflection is noticeably enlarged with the increase of the nondimensional ISW amplitude, meaning that more energy might be allocated on such response. As a result, less energy concentrates on the IL VIV response, causing the decrease of maximum VIV amplitude in the IL direction. As for the maximum CF VIV amplitude, the increase of the nondimensional ISW amplitude can barely exert an influence on its value, which can be attributed to the reduced velocity for CF VIV response. It should be mentioned that the excited modes of VIV in both IL and CF directions show an increasing trend with the increase of the nondimensional ISW amplitude in Fig. 12, which is consistent with the analyses in Sec. IV B. It should be mentioned that the summation of multi-frequency VIV responses and

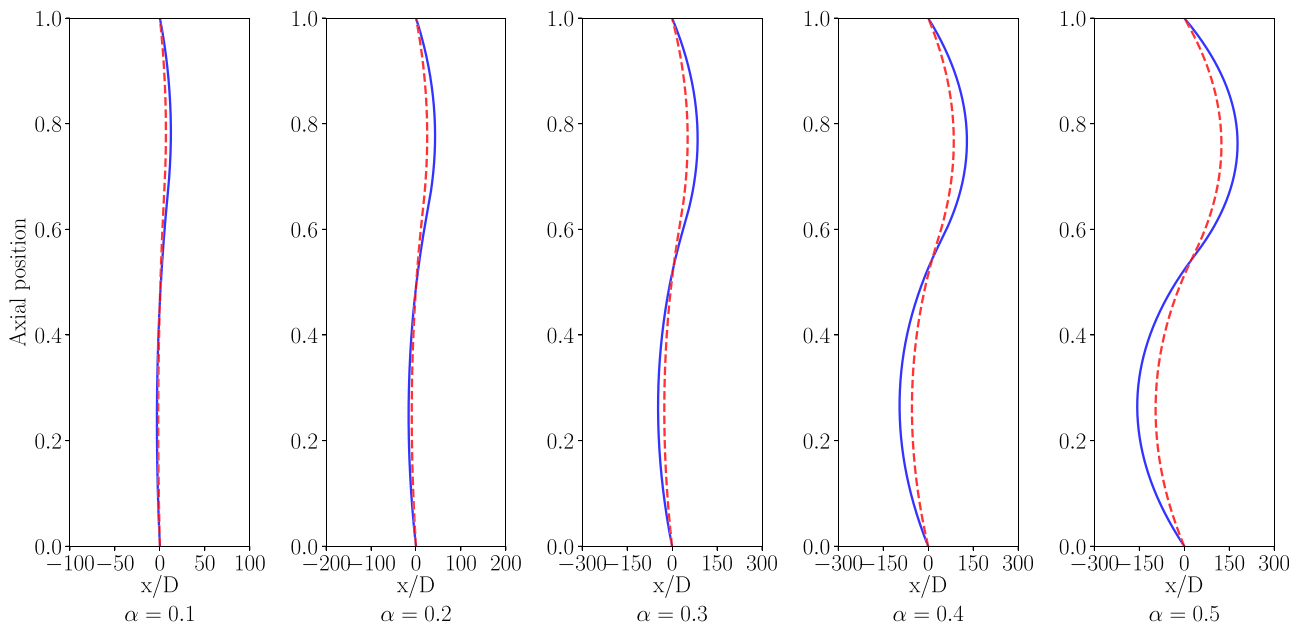


FIG. 11. Inline deflection along the flexible riser with various nondimensional ISW amplitudes (blue: with VIV and red: without VIV).

08 April 2024 02:58:45

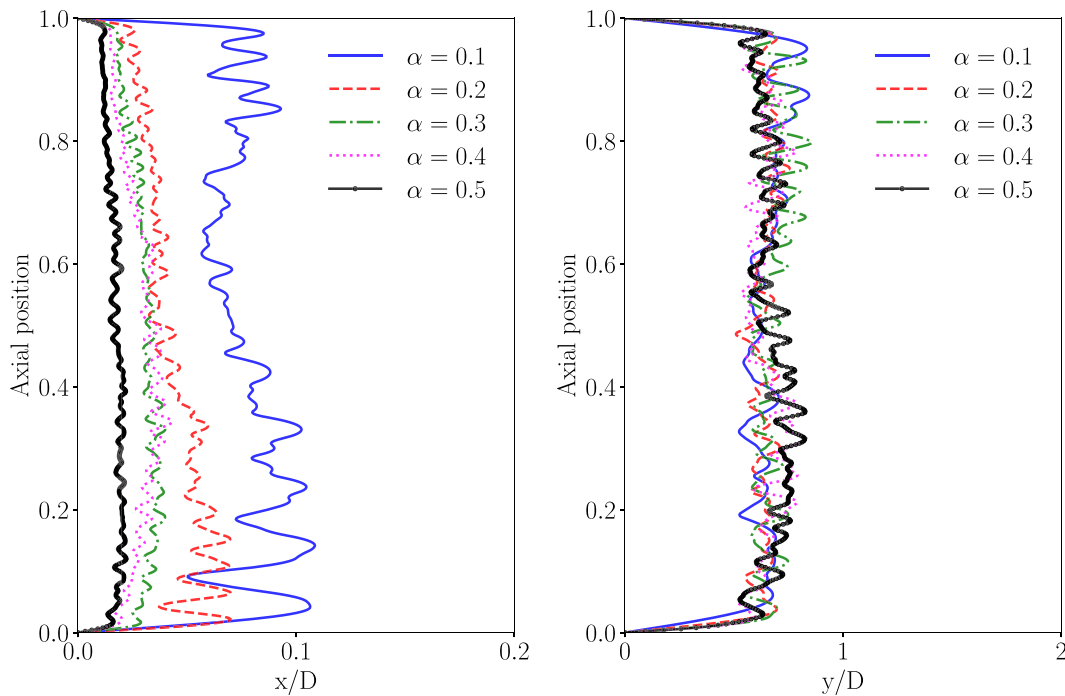


FIG. 12. Maximum VIV amplitudes along the flexible riser in IL and CF directions with various nondimensional ISW amplitudes.

the transient duration of each mode VIV response can also contribute to the variation of IL and CF VIV amplitudes with the increase of the nondimensional ISW amplitude.

When VIV can be triggered by ISW, the maximum inline deflection can be also influenced by VIV via affecting the drag force. It is proved that the drag coefficient can be impacted and closely related to VIV amplitude in the CF direction by Vandier,⁶² where the drag coefficient $C_D = C_{D0}[1 + 1.043(2y_{RMS}/D)^{0.65}]$ is affected by the variation of vibration amplitude ($C_{D0} = 1.2$, and y_{RMS} and D denote the root mean square displacement in CF direction and riser diameter, respectively). Hence, the maximum inline deflection can be changed by the existence of VIV response. Regardless of the nondimensional ISW amplitude, the maximum inline deflection with consideration of VIV response is evidently larger than that with the absence of VIV, as shown in Fig. 11. For example, without the effect of VIV, the maximum inline deflection under the nondimensional ISW amplitude $\alpha = 0.1$ is found equal to approximately 6.72 and 1.88 for the upper and lower sections while the maximum inline deflections of around 123.98 and 95.67 with $\alpha = 0.5$ can be captured in the upper and lower layers, respectively. Compared with those considering VIV response above, the values of maximum inline deflection without VIV are notably small. This is because when VIV occurs, the drag coefficient is enlarged due to the existence of CF VIV response. As a consequence, the drag force is increased, resulting in the magnification of the maximum inline deflection. It can be also observed from Fig. 11 that the enlargement of the maximum inline deflection tends to be intensive with the increase of the nondimensional ISW amplitude, which can be attributed to the combination effect of CF VIV response and amplified induced velocity by ISW.

F. Maximum stress along the flexible riser

Since the changes of the inline deflection and VIV responses can contribute to the variation of the stress along the flexible riser, the maximum riser stress in IL direction is mainly calculated and depicted in Fig. 13 while the nondimensional ISW amplitude is increased. It can be found that when the effect of IL and CF VIV responses on the stress along the flexible riser is taken into account, the maximum stress values on both upper and lower sections are noticeably increased regardless of the nondimensional ISW amplitude. As shown in Fig. 13, with the nondimensional ISW amplitude $\alpha = 0.1$, the maximum stress values without VIV are equal to about 15.24 and 4.20 MPa on the upper and lower sections, respectively, while the maximum stress values of around 30.36 and 7.84 MPa can be detected with the consideration of VIV. This is because the combination effect of VIV responses and the enlarged inline deflection due to VIV is responsible for the increase of maximum stress along the flexible riser. In addition, the maximum stress on the upper section of the flexible is larger compared with that on the lower section due to higher flow velocity induced by ISW in the upper layer.

In terms of the nondimensional ISW amplitude effect, the maximum value of the stress along the flexible riser shows a remarkably increasing trend with or without VIV while the nondimensional ISW amplitude is increased. It can be observed from Fig. 13 that as the nondimensional ISW amplitude is up to 0.5, the maximum stresses on the upper and lower sections are enlarged to approximately 227.04 and 173 MPa, respectively, with the absence of VIV effect. Meanwhile, when the effect of VIV is taken into account, the maximum values of about 357.30 and 269.14 MPa are captured for the riser stress on these two sections under $\alpha = 0.5$. The enlargement of maximum stress

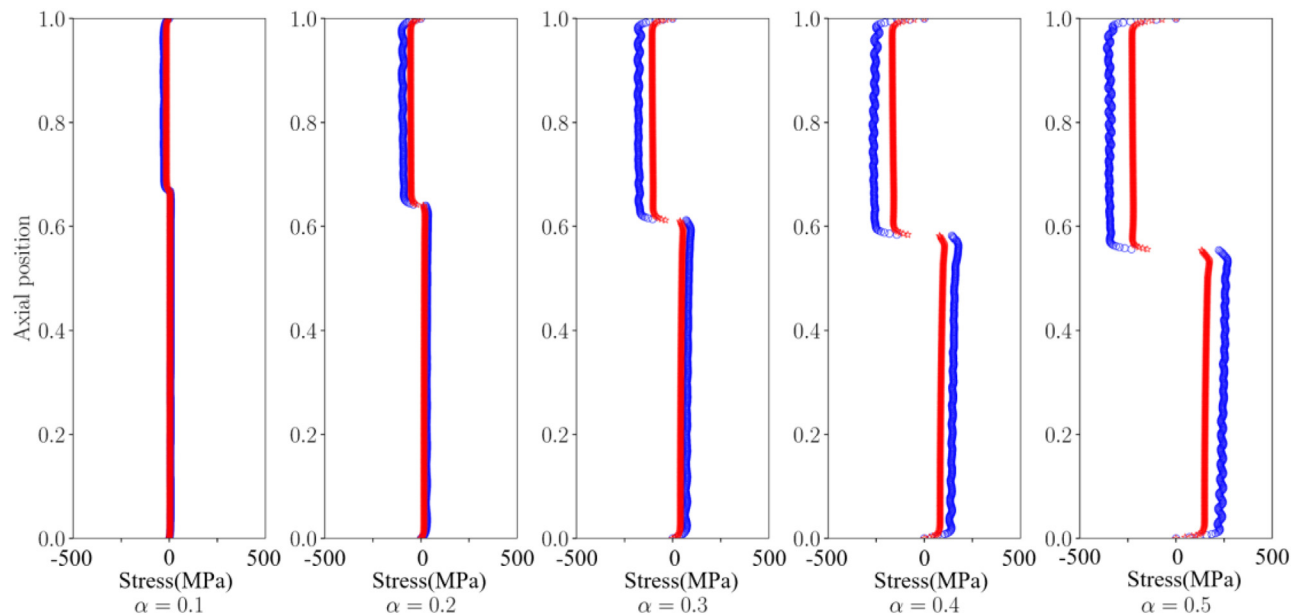


FIG. 13. Maximum stress along the flexible riser with various nondimensional ISW amplitudes (blue: with VIV and red: without VIV).

values can be explained by the effect of inline deflection and VIV responses, particularly by the inline deflection magnification.

Another characteristic worthy attention is that the VIV responses can have an effect on the stress distribution along the flexible riser. It can be seen from Fig. 13 that the maximum stress distribution along the flexible riser is characterized with fluctuation on both upper and lower sections, which can be ascribed to the effect of VIV responses. Moreover, with the increase of the nondimensional ISW amplitude, the fluctuation of the maximum stress along the flexible riser tends to be more conspicuous.

V. CONCLUSIONS

The dynamic response of a flexible riser undergoing ISW is investigated considering the effect of the nondimensional ISW amplitude. First, the applied models of the flexible riser, ISW, and hydrodynamic force are elaborated. Then, validations are carried out based on the comparison between numerical results and experimental data so that the accuracy of the models can be guaranteed, in particular, for the ISW generation model. Afterward, the effect of the nondimensional ISW amplitude on the dynamic response of the full-scale flexible riser is examined. The changes in VIV oscillation frequencies and amplitudes in both IL and CF directions, top tension, inline deflection, and stress along the flexible riser are mainly explored with the increase of the nondimensional ISW amplitude.

It is found that multi-mode and multi-frequency IL and CF VIV responses can be excited with the propagation of ISW. The values of VIV amplitudes vary with the ISW propagation and hysteresis caused by ISW can be captured for IL and CF VIV. Due to the discrepancy of the induced velocities by ISW in the upper and lower layers, the maximum values of oscillation frequencies, inline deflection, as well as stress on the upper section of the flexible riser are found larger

compared with those on the lower section. In addition, VIV responses can exert an impact on the top tension, inline deflection, and stress along the flexible riser.

With the increase of the nondimensional ISW amplitude, high mode VIV responses accompanied by high vibration frequencies can be triggered in both IL and CF directions while the ISW trough passes through the flexible riser. When the nondimensional ISW amplitude is increased, the maximum VIV amplitude in the IL direction shows a decreasing trend while the maximum CF VIV amplitude is hardly changed. In addition, the nondimensional ISW amplitude increase can enhance the maximum values of top tension, inline deflections, as well as stress along the flexible riser noticeably.

Here, the dynamic response of a full-scale flexible riser subjected to ISW has been investigated with the consideration of the nondimensional ISW amplitude effect. Correspondingly, the characteristics and mechanism of IL and CF VIV responses, top tension, as well as stress along the flexible riser have been analyzed and revealed. Nevertheless, more research on the dynamic response of the flexible riser undergoing ISW should be carried out while other factors are taken into account, such as the background current and wave as well as vessel motion.

ACKNOWLEDGMENTS

The work was supported by the National Natural Science Foundation of China (Grant Nos. 12202455, 12132018, and 11972352) and the Strategic Priority Research Program of the Chinese Academy of Sciences (Grant No. XDA22040304). Insightful advice from Dr. Changhong Zhi at Shanghai Jiao Tong University and Dr. Zian Wang at Institute of Mechanics, Chinese Academy of Sciences is also gratefully acknowledged.

AUTHOR DECLARATIONS

Conflict of Interest

The authors have no conflicts to disclose.

Author Contributions

Jinlong Duan: Conceptualization (equal); Data curation (equal); Formal analysis (equal); Funding acquisition (equal); Investigation (equal); Methodology (equal); Software (equal); Validation (equal); Visualization (equal); Writing – original draft (equal); Writing – review & editing (equal). **Xu Wang:** Funding acquisition (equal); Methodology (equal); Project administration (equal); Resources (equal); Software (equal). **Jifu Zhou:** Conceptualization (equal); Funding acquisition (equal); Methodology (equal); Resources (equal); Supervision (equal); Visualization (equal); Writing – review & editing (equal). **Yunxiang You:** Conceptualization (equal); Methodology (equal).

DATA AVAILABILITY

The data that support the findings of this study are available from the corresponding author upon reasonable request.

REFERENCES

- ¹A. K. Liu, Y. S. Chang, M.-K. Hsu, and N. K. Liang, “Evolution of nonlinear internal waves in the east and South China Seas,” *J. Geophys. Res.* **103**(C4), 7995–8008, <https://doi.org/10.1029/97JC01918> (1998).
- ²J. M. Klymak, R. Pinkel, C.-T. Liu, A. K. Liu, and L. David, “Prototypical solitons in the South China Sea,” *Geophys. Res. Lett.* **33**(11), L11607, <https://doi.org/10.1029/2006GL025932> (2006).
- ³M. H. Alford, R.-C. Lien, H. Simmons, J. M. Klymak, S. Ramp, Y. J. Yang *et al.*, “Speed and evolution of nonlinear internal waves transiting the South China Sea,” *J. Phys. Oceanogr.* **40**(6), 1338–1355 (2010).
- ⁴S. Cai, J. Xie, and J. He, “An overview of internal solitary waves in the South China Sea,” *Surv. Geophys.* **33**(5), 927–943 (2012).
- ⁵Z. Tian, Y. Jia, J. Chen *et al.*, “Internal solitary waves induced deep-water nepheloid layers and seafloor geomorphic changes on the continental slope of the northern South China Sea,” *Phys. Fluids* **33**(5), 053312 (2021).
- ⁶R. C. Lien, F. Henyey, B. Ma, and Y. J. Yang, “Large-amplitude internal solitary waves observed in the northern South China Sea: Properties and energetics,” *J. Phys. Oceanogr.* **44**(4), 1095–1115 (2014).
- ⁷M. H. Alford, T. Peacock, J. A. MacKinnon *et al.*, “The formation and fate of internal waves in the South China Sea,” *Nature* **521**, 65–69 (2015).
- ⁸X. D. Huang, Z. H. Chen, W. Zhao *et al.*, “An extreme internal solitary wave event observed in the northern South China Sea,” *Sci. Rep.* **6**, 30041 (2016).
- ⁹J. Xu, Y. He, Z. Chen, H. Zhan *et al.*, “Observations of different effects of an anti-cyclonic eddy on internal solitary waves in the South China Sea,” *Prog. Oceanogr.* **188**, 102422 (2020).
- ¹⁰P. Hyder, D. R. G. Jeans, E. Cauquil, and R. Nerzic, “Observations and predictability of internal solitons in the northern Andaman Sea,” *Appl. Ocean Res.* **27**(1), 1–11 (2005).
- ¹¹A. K. Liu, S. R. Ramp, Y. Zhao, and T. Y. Tang, “A case study of internal solitary wave propagation during ASIAEX 2001,” *IEEE J. Ocean. Eng.* **29**(4), 1144–1156 (2004).
- ¹²E. L. Shroyer, J. N. Moum, and J. D. Nash, “Observations of polarity reversal in shoaling nonlinear internal waves,” *J. Phys. Oceanogr.* **39**(3), 691–701 (2009).
- ¹³K. H. Fu, Y. H. Wang, L. S. Laurent, H. Simmons, and D. P. Wang, “Shoaling of large amplitude nonlinear internal waves at Dongsha Atoll in the northern South China Sea,” *Cont. Shelf Res.* **37**(37), 1–7 (2012).
- ¹⁴R. Grimshaw, K. R. Helfrich, and E. R. Johnson, “Experimental study of the effect of rotation on large amplitude internal waves,” *Phys. Fluids* **25**(5), 056602 (2013).
- ¹⁵X. Bai, Z. Liu, Q. Zheng, J. Hu, K. G. Lamb, and S. Cai, “Fission of shoaling internal waves on the northeastern shelf of the South China Sea,” *J. Geophys. Res.* **124**(7), 4529–4545, <https://doi.org/10.1029/2018JC014437> (2019).
- ¹⁶Z. Wen, L. Zou, Y. Hu *et al.*, “Numerical study on the surface signature of internal solitary waves,” *Phys. Fluids* **34**(7), 072105 (2022).
- ¹⁷A. S. Dosaev, M. I. Shishina, and Y. I. Troitskaya, “Numerical simulation of solitary gravity waves on deep water with constant vorticity,” *Phys. Fluids* **34**(9), 092101 (2022).
- ¹⁸H. Du, G. Wei, M. Gu *et al.*, “Experimental investigation of the load exerted by nonstationary internal solitary waves on a submerged slender body over a slope,” *Appl. Ocean Res.* **59**, 216–223 (2005).
- ¹⁹J. Xie, J. Xu, and S. Cai, “A numerical study of the load on cylindrical piles exerted by internal solitary waves,” *J. Fluids Struct.* **27**(8), 1252–1261 (2011).
- ²⁰X. Wang, J. F. Zhou, Z. Wang *et al.*, “A numerical and experimental study of internal solitary wave loads on semi-submersible platforms,” *Ocean Eng.* **150**, 298–308 (2018).
- ²¹S. Cai, J. Xu, Z. Chen *et al.*, “The effect of a seasonal stratification variation on the load exerted by internal solitary waves on a cylindrical pile,” *Acta Oceanol. Sin.* **33**(7), 21–26 (2014).
- ²²X. Wang, J. F. Zhou, Z. Wang *et al.*, “A numerical and experimental study of internal solitary wave loads on semi-submersible platforms,” *Ocean Eng.* **150**, 298–308 (2018).
- ²³M. Chen, K. Chen, Y. X. You *et al.*, “Experimental study of forces on a multi-column floating platform in internal solitary waves,” *Appl. Ocean Res.* **78**, 192–200 (2018).
- ²⁴F. Wang, H. Guo, X. Li *et al.*, “Experimental study on ocean internal wave force on vertical cylinders in different depths,” *China Ocean Eng.* **30**(3), 459–468 (2016).
- ²⁵F. Wang, R. Sun, C. Wang *et al.*, “Experimental study on flow field induced by internal solitary wave and load characteristics on pile sections at different depth,” *Ocean Eng.* **188**, 106292 (2019).
- ²⁶S. Cai, S. Wang, and X. Long, “A simple estimation of the force exerted by internal solitons on cylindrical piles,” *Ocean Eng.* **33**, 974–980 (2006).
- ²⁷S. Q. Cai, X. M. Long, and S. G. Wang, “Forces and torques exerted by internal solitons in shear flows on cylindrical piles,” *Appl. Ocean Res.* **30**(1), 72–77 (2008).
- ²⁸J. Xie, Y. Jian, and L. Yang, “Strongly nonlinear internal soliton load on a small vertical circular cylinder in two-layer fluids,” *Appl. Math. Model.* **34**, 2089–2101 (2010).
- ²⁹Z. Song, B. Teng, Y. Gou, L. Lu, Z. Shi, Y. Xiao *et al.*, “Comparisons of internal solitary wave and surface wave actions on marine structures and their responses,” *Appl. Ocean Res.* **33**, 120–129 (2011).
- ³⁰Z. Si, Y. Zhang, and Z. Fan, “A numerical simulation of shear forces and torques exerted by large-amplitude internal solitary waves on a rigid pile in South China Sea,” *Appl. Ocean Res.* **37**, 127–132 (2012).
- ³¹Z. Xu, B. Yin, H. Yang, and J. Qi, “Depression and elevation internal solitary waves in a two-layer fluid and their forces on cylindrical piles,” *Chin. J. Oceanol. Limnol.* **30**, 703–712 (2012).
- ³²H. Lü, J. Xie, J. Xu, Z. Chen, T. Liu, and S. Cai, “Force and torque exerted by internal solitary waves in background parabolic current on cylindrical tendon leg by numerical simulation,” *Ocean Eng.* **114**, 250–258 (2016).
- ³³E. Ermanyuk and N. Gavrilov, “Experimental study of the dynamic effect of an internal solitary wave on a submerged circular cylinder,” *J. Appl. Mech. Tech. Phys.* **46**, 800–806 (2005).
- ³⁴Y. Wang, L. Wang, H. Zhu, H. Tang, and G. Wei, “A numerical study of the forces on two tandem cylinders exerted by internal solitary waves,” *Math. Probl. Eng.* **2016**, 9086246 (2016).
- ³⁵W. Yin, H. Guo, K. Wu, and D. Ma, “Calculation of internal solitary wave force on horizontal submerged circular cylinder,” *J. Zhejiang Univ. Eng. Sci.* **50**(7), 1252 (2016).
- ³⁶W. Ding, C. Ai, S. Jin, and J. Lin, “3D numerical investigation of forces and flow field around the semi-submersible platform in an internal solitary wave,” *Water* **12**, 208 (2020).
- ³⁷S. D. Wang, G. Wei, H. Du *et al.*, “Experimental investigation of the wave-flow structure of an oblique internal solitary wave and its force exerted on a slender body,” *Ocean Eng.* **201**, 107057 (2020).
- ³⁸M. Chen, K. Chen, and Y. X. You, “Experimental investigation of internal solitary wave forces on a semi-submersible,” *Ocean Eng.* **141**, 205–214 (2017).
- ³⁹J. Cui, S. Dong, Z. Wang, X. Han, and M. Yu, “Experimental research on internal solitary waves interacting with moored floating structures,” *Mar. Struct.* **67**, 102641 (2019).

- ⁴⁰S. Cheng, Y. Yu, Z. Li *et al.*, “The influence of internal solitary wave on semi-submersible platform system including mooring line failure,” *Ocean Eng.* **258**, 111604 (2022).
- ⁴¹P. X. Zou, J. D. Bricker, and W. S. J. Uijtewaal, “The impacts of internal solitary waves on a submerged floating tunnel,” *Ocean Eng.* **238**, 109762 (2021).
- ⁴²Y. Gong, H. Song, Z. Zhao *et al.*, “On the vertical structure of internal solitary waves in the northeastern South China Sea,” *Deep Sea Res. Part I* **173**, 103550 (2021).
- ⁴³J. Zhang, Y. Liu, K. Chen *et al.*, “Experimental study of internal solitary wave loads on the semi-submersible platform,” *Int. J. Nav. Archit. Ocean Eng.* **13**, 718–733 (2021).
- ⁴⁴Z. Zhai, S. Zheng, and D. Wan, “Interaction between solitary waves and a combined structure of two concentric asymmetric porous arc walls,” *Phys. Fluids* **34**(4), 042103 (2022).
- ⁴⁵P. Peng, H. Du, G. Wei *et al.*, “Experimental investigation on the vertical structure characteristics of internal solitary waves,” *J. Mar. Sci. Eng.* **10**(8), 1045 (2022).
- ⁴⁶L. Zhang, H. Guo, and F. Meng, “Investigation on the dynamic responses of vertical cylinder undergoing internal waves,” in *Twenty-Third International Offshore and Polar Engineering Conference* (OnePetro, 2013).
- ⁴⁷H. Y. Guo, L. Zhang, and X. M. Li, “Dynamic responses of top tensioned riser under combined excitation of internal solitary wave, surface wave and vessel motion,” *J. Ocean Univ. China* **12**(1), 6–12 (2013).
- ⁴⁸M. Lou and C. Yu, “Dynamic responses of a riser under combined excitation of internal waves and background currents,” *Int. J. Naval Archit. Ocean Eng.* **6**(3), 685–699 (2014).
- ⁴⁹S. Deng, C. Li, H. Fan *et al.*, “Impact evaluation of internal solitary waves on a drilling riser,” in *Twenty-fifth International Ocean and Polar Engineering Conference (ISOPE-I)* (OnePetro, 2015), pp. 15–685.
- ⁵⁰H. Fan, C. Li, Z. Wang *et al.*, “Dynamic analysis of a hang-off drilling riser considering internal solitary wave and vessel motion,” *J. Nat. Gas Sci. Eng.* **37**, 512–522 (2017).
- ⁵¹J. Zhang, Y. Zeng, Y. Tang *et al.*, “Numerical and experimental research on the effect of platform heave motion on vortex-induced vibration of deep sea top-tensioned riser,” *Shock Vib.* **2021**, 8866051 (2021).
- ⁵²R. Wang, G. Chen, X. Liu *et al.*, “Safety analysis of deep-sea mining pipeline deployment operations considering internal solitary waves,” *Mar. Georesour. Geotechnol.* **40**(2), 125–138 (2022).
- ⁵³H. Gu, H. Guo, X. Li *et al.*, “Three-dimensional dynamic analysis of deep-water steel steep wave riser considering internal solitary wave,” *J. Mar. Sci. Technol.* **27**(1), 452–466 (2022).
- ⁵⁴L. Guo, M. Duan, and Z. Zhu, “A dynamic model of deep water riser and its global response characteristics induced by ocean internal wave and floating platform,” *Ships Offshore Struct.* **17**(7), 1592–1603 (2022).
- ⁵⁵K. R. Helfrich and W. K. Melville, “Long nonlinear internal waves,” *Annu. Rev. Fluid Mech.* **38**(1), 395–425 (2006).
- ⁵⁶J. Grue, A. Jensen, P. O. Rusås *et al.*, “Properties of large-amplitude internal waves,” *J. Fluid Mech.* **380**, 257–278 (1999).
- ⁵⁷J. Duan, J. Zhou, Y. You *et al.*, “Time-domain analysis of vortex-induced vibration of a flexible mining riser transporting flow with various velocities and densities,” *Ocean Eng.* **220**, 108427 (2021).
- ⁵⁸J. Duan, J. Zhou, Y. You *et al.*, “Effect of internal flow on vortex-induced vibration dynamics of a flexible mining riser in external shear current,” *Mar. Struct.* **80**, 103094 (2021).
- ⁵⁹J. Duan, J. Zhou, X. Wang *et al.*, “Cross-flow vortex-induced vibration of a flexible fluid-conveying riser undergoing external oscillatory flow,” *Ocean Eng.* **250**, 111030 (2022).
- ⁶⁰J. Duan, J. Zhou, X. Wang *et al.*, “Vortex-induced vibration of a flexible fluid-conveying riser due to vessel motion,” *Int. J. Mech. Sci.* **223**, 107288 (2022).
- ⁶¹S. X. Fu, J. G. Wang, R. Baarholm, J. Wu, and C. M. Larsen, “Features of vortex-induced vibration in oscillatory flow,” *J. Offshore Mech. Arct. Eng.* **136**(1), 011801 (2014).
- ⁶²J. K. Vandiver, “Drag coefficients of long flexible cylinders,” paper presented at the Offshore Technology Conference, Houston, Texas, USA, 1983.